Materials Science & Engineering A 690 (2017) 104–119

Contents lists available at ScienceDirect

Materials Science & Engineering A

journal homepage: www.elsevier.com/locate/msea

Tensile mechanical properties, constitutive equations, and fracture mechanisms of a novel 9% chromium tempered martensitic steel at elevated temperatures

Bo Xiao[a,b], Lianyong Xu[a,b,*], Lei Zhao[a,b], Hongyang Jing[a,b], Yongdian Han[a,b]

[a] School of Materials Science and Engineering, Tianjin University, Tianjin 300072, China
[b] Tianjin Key Laboratory of Advanced Joining Technology, Tianjin 300072, China

ARTICLE INFO

Keywords:
G115 steel
Tensile behavior
Fracture mechanism
Constitutive equation
Microstructures

ABSTRACT

To explore the high-temperature tensile behavior and fracture mechanism of a novel 9% chromium tempered martensitic steel, G115, a series of tensile tests were conducted at 625, 650, and 675 °C within the strain rate range of 5.2×10^{-5}–5.2×10^{-3} s^{-1}. The results demonstrated that the tensile strength decreased with increasing temperature and decreasing strain rate. However, the elongation to failure increased with increasing temperature. The ductility at 675 °C exhibited significant improvement. Furthermore, three typical constitutive equations were comparatively analyzed to accurately describe the tensile deformation behavior of G115 steel. A stress exponent of approximately 11.1 and an activation energy of approximately 639.865 kJ/mol were obtained via the hyperbolic sine law. To explain the actual deformation mechanism, the threshold stress concept was introduced. The modified hyperbolic sine constitutive equation was proposed to determine the threshold stress σ_{th}, the true stress exponent n^t, and the true activation energy Q^t of G115 steel. The Q^t value increased with increasing temperature and strain rate. Dislocation climb was the dominant deformation mechanism under the tested conditions. In addition, fracture surface investigations revealed a typical ductile fracture mode with a dense array of dimples at 625 and 650 °C. However, transgranular facets with tear ridges were observed in the central region at 675 °C. In addition, the microstructures of the fracture frontier and longitudinal section away from the fracture surface were studied to further understand the fracture mechanism.

1. Introduction

Ultra-supercritical (USC) power plants exhibit improved thermal efficiency because of increased steam temperature and pressure [1,2]. Hence, the continuous exhaustion of fossil resources and the effects of environmental pollution worldwide make it urgently necessary for power plants to operate under USC conditions [3–6]. In recent years, 9–12% chromium martensitic heat-resistant steels have been broadly applied in USC coal-fired power plants [7–11] owing to their excellent creep properties. However, conventional martensitic heat-resistant steels, such as P92 [12–14] and P122 steel [15–17], rapidly lose strength at temperatures above 650 °C due to recrystallization, precipitate coarsening, and dissolution at higher temperatures, and can no longer meet the requirements under higher-temperature conditions.

For these reasons, many efforts have been made to develop higher-grade martensitic steels. 9Cr–3W–3Co steels, which were first developed by the National Institute of Materials Science in Japan, are expected to be used at 650 °C [18]. Numerous studies have been conducted on 9Cr–3W–3Co steels, such as studies of the alloy design [19,20], microstructure evolution [21,22], and creep behavior at elevated temperatures [23–25]. Interestingly, a novel, tempered martensitic heat-resistant steel, G115, with improved creep properties at elevated temperatures has been developed by the China Iron and Steel Research Institute [26–30] and will potentially be used in USC power plants at temperatures up to 650 °C. To date, only a few characteristics of this steel have been studied, such as the effect of heat treatment on the strength [27,28], the evolution of the microstructure and toughness during aging [26,30], and various others [29]. Furthermore, understanding the high-temperature tensile behavior and fracture mechanism of G115 steel are also essential to comprehending the relationship between its high-temperature tensile deformation behavior and fracture mechanism; this will provide important data to verify the reliability of G115 steel for future applications.

However, limited work has been done on the high-temperature tensile behavior and fracture mechanism of G115 steel. Therefore, in this study, these features were compared at various elevated tempera-

* Corresponding author at: School of Materials Science and Engineering, Tianjin University, Tianjin 300072, China.
E-mail address: xulianyong@tju.edu.cn (L. Xu).

http://dx.doi.org/10.1016/j.msea.2017.02.099
Received 6 January 2017; Received in revised form 24 February 2017; Accepted 25 February 2017
Available online 28 February 2017

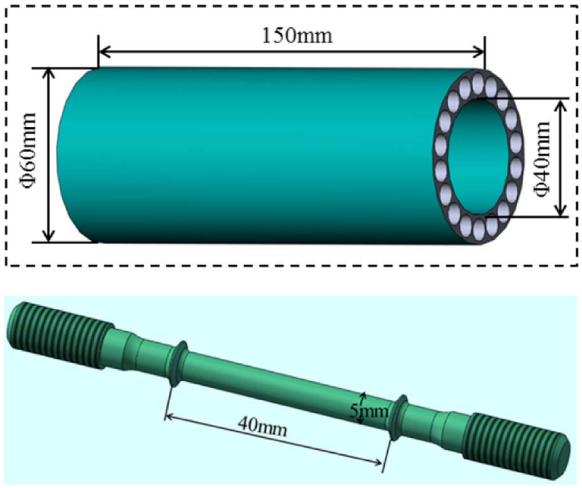

Fig. 1. Shape of the original material and schematic of the test specimens.

Table 1
Chemical composition (wt%) of the as-received G115 steel.

Element	C	Cr	W	Co	Cu	Mn	Si	V	Nb	N	B	Fe
Amount	0.08	8.8	2.8	3.0	1.0	0.5	0.3	0.2	0.06	0.008	0.014	Bal.

Fig. 2. Optical micrograph showing tempered martensitic microstructure of the as-received G115 steel.

tures (625–675 °C) and strain rates (5.2×10^{-5}–5.2×10^{-3} s^{-1}). On the basis of the experimental results, the optimum constitutive equation to accurately describe the flow behavior was derived, and the high-temperature deformation mechanism was analyzed via the hyperbolic sine law, along with the threshold stress and Young's modulus. Furthermore, to better understand the fracture mechanism of G115 steel, the fracture characteristics, microstructures at the fracture frontier, and microstructures away from the fracture surface of ruptured specimens were also studied.

2. Experimental procedures

2.1. Material

In this study, G115 steel was selected as the experimental material. The original material was in pipe form, with an outer diameter of 60.0 mm and a thickness of 10.0 mm (Fig. 1). Its chemical composition is listed in Table 1. The steel was normalized at 1100 °C for 1 h and then tempered at 760 °C for 3 h.

2.2. Microstructural characterization

Metallographic analyses were conducted via optical microscopy (OM, Axio Vert A1). The fracture surfaces were analyzed via scanning electron microscopy (SEM, ZEISS EVO 18) to determine the fracture mechanism. The samples for the OM and SEM examinations were prepared by standard mechanical polishing procedures and then etched in a mixed solution (5 g $FeCl_3$+15 ml HCl+80 ml H_2O) for 35 s. As G115 steel is a novel material, it is necessary to determine its precipitates and dislocation structure. Therefore, the microstructures of the as-received material were analyzed using transmission electron microscopy (TEM, Tecnai G2 F30) coupled with energy-dispersive spectroscopy.

2.3. Tensile tests

All tensile tests were performed using a tensile testing machine equipped with an elevated temperature furnace and an extensometer. Tests were conducted on standard tensile specimens with a gage diameter of 5.0 mm and gage length of 40.0 mm (Fig. 1). All standard tensile specimens were cut along the longitudinal axial direction of the original material. Details of the positions and dimensions of the tensile specimens are shown in Fig. 1. High-temperature tensile tests were performed at temperatures ranging from 625 to 675 °C and strain rates ranging from 5.2×10^{-5} to 5.2×10^{-3} s^{-1}. The temperature along the specimen was controlled with a tolerance of ± 1 °C. The holding time before the start of the tensile test was approximately 60 min. The yield strength (YS) was determined from the 0.2% offset flow stress.

3. Results and discussion

3.1. Microstructural characteristics

Fig. 2 shows an OM image of the as-received G115 steel. The tempered martensitic structure appears in the microstructure of the steel. The average size of the prior austenite grains was estimated to be appropriately 50 μm.

Fig. 3 shows TEM images of the as-received steel. Martensitic laths with high dislocation density are visible in Fig. 3a, which shows that a significant amount of precipitates nucleated on the lath boundaries or within the micrograins. Fig. 3b shows the cell structure, which, interestingly, resulted from dislocation entanglement. Two types of precipitates can be distinguished: $M_{23}C_6$ and MX, as shown in Fig. 3c and d, respectively. The $M_{23}C_6$ type has an ellipsoidal shape and a size of ~150 nm and is located mainly on the prior austenite grains and martensitic lath boundaries. The MX type is square and ~40 nm in size, and is distributed mainly along the martensitic lath.

3.2. Engineering stress–strain curves

Engineering stress–strain curves of the G115 steel under various conditions were plotted from the data recorded during the tests (Fig. 4). The flow stress is sensitive to both strain rate and temperature. Under constant strain rate conditions, a decrease in flow stress is observed when the temperature increases (Fig. 4a–c). Similarly, under constant temperature conditions, the flow stress increases with increasing strain rate (Fig. 4d–f). In addition, there is no obvious transition from the yield point to the peak in any of the tensile curves, indicating continuous yielding and good formability of the steel. Furthermore, on the basis of the shape of the engineering stress–strain curves, the tensile curve can be divided into three stages [31], as shown in Fig. 5. Three regions appear: in Stage I, the flow stress increases with increasing strain (from point zero to point P). Stage II is characterized